Self-Similar Multimode Bubble-Front Evolution of the Ablative Rayleigh-Taylor Instability in Two and Three Dimensions

H. Zhang,[1,2,*] R. Betti,[1,2] R. Yan,[3] D. Zhao,[1,2] D. Shvarts,[4] and H. Aluie[1,2]
[1]Department of Mechanical Engineering, University of Rochester, Rochester, New York 14627, USA
[2]Laboratory for Laser Energetics, University of Rochester, Rochester, New York 14627, USA
[3]Department of Modern Mechanics, University of Science and Technology of China, Hefei 230026, China
[4]Department of Physics, NRCN, Beer Sheva, Israel

(Received 19 April 2018; revised manuscript received 31 July 2018; published 31 October 2018)

The self-similar nonlinear evolution of the multimode ablative Rayleigh-Taylor instability (ARTI) is studied numerically in both two and three dimensions. It is shown that the nonlinear multimode bubble-front penetration follows the $\alpha_b A_T (\int \sqrt{g} dt)^2$ scaling law with α_b dependent on the initial conditions and ablation velocity. The value of α_b is determined by the bubble competition theory, indicating that mass ablation reduces α_b with respect to the classical value for the same initial perturbation amplitude. It is also shown that ablation-driven vorticity accelerates the bubble velocity and prevents the transition from the bubble competition to the bubble merger regime at large initial amplitudes leading to higher α_b than in the classical case. Because of the dependence of α_b on initial perturbation and vorticity generation, ablative stabilization of the nonlinear ARTI is not as effective as previously anticipated for large initial perturbations.

DOI: 10.1103/PhysRevLett.121.185002

The Rayleigh-Taylor instability (RTI) occurs when a heavy fluid is accelerated against a light fluid [1,2]. It develops in a multitude of natural and engineering systems, such as jet-driven lobes in the intergalactic cluster [3], supernova explosions [4], and inertial confinement fusion (ICF) [5]. In ICF, a low-density hot plasma pushes on the cold dense shell and the RTI growth is affected by mass ablation off the unstable interface. In this case, the RTI is often referred to as ablative RTI (ARTI) as opposed to the classical RTI (CRTI) of two superimposed inviscid fluids. In ICF implosions, the ARTI seeded by short wavelength target surface roughness or laser imprint [6] can severely degrade the implosion performance and prevent thermonuclear ignition of the fusion fuel. ARTI also plays a central role in the evolution of supernova (SN) explosions, where it is the dominant process accelerating the deflagration front [7].

The RTI perturbations usually consist of multiple modes. The nonlinear RTI theory predicts that the multimode interaction can reach a self-similar regime with the bubble penetration distance $h_b = \alpha_b A_T S$ [8]. Here $S = (\int \sqrt{g} dt)^2$, g is the time-dependent acceleration, $A_T = (\rho_h - \rho_l)/(\rho_h + \rho_l)$ is the Atwood number, ρ_h and ρ_l are the density of the heavy and light fluids. In the constant acceleration limit, $h_b = \alpha_b A_T g_o t^2$ [9–11]. The coefficient α_b is expected to be constant in time and its value determines the nonlinear evolution of the RTI. For instance, the value of α_b is crucial to resolving the long-standing question of whether deflagration alone can account for an SN explosion, or if detonation is required [12]. Moreover, α_b determines the mixing rate of the radioactive material in supernova ejecta, which is further invoked to explain the measured light emission curves [13]. In a successful ICF implosion, the RTI bubble penetration ($\alpha_b A_T S$) must be less than the in-flight shell thickness (Δ) to prevent shell breakup [14–16]. The importance of α_b in ICF is also manifested through the minimum kinetic energy ($\mathrm{KE}_{\mathrm{min}}^{ig}$) required for ignition that scales as $\mathrm{KE}_{\mathrm{min}}^{ig} \sim \alpha_b^3$ [17,18]. A more unstable implosion would require a kinetic energy increasing like α_b^3. Nonlinear RTI and its growth rate α_b are also important in many other systems, such as neutron stars [19], photo-evaporated interstellar clouds such as the Eagle Nebula [20], overturning circulation in the ocean and atmosphere [21], and tokamak stability [22]. Theoretically, self-similarity can be achieved in two limiting ways, i.e., bubble merger [9,23] and bubble competition [24,25]. The former regime is insensitive to the initial condition and a universal α_b value is expected. In the latter regime, α_b increases logarithmically with the initial perturbation amplitude h_0 and can be approximated by [10]

$$\alpha_b \approx \frac{C\sqrt{\pi}}{4}\left(\ln\frac{2C\sqrt{\pi}}{k_0 h_0} - 1\right)^{-1}. \tag{1}$$

The coefficient C and k_0 are two parameters determined by comparing with experiments or simulations.

CRTI experiments show $\alpha_b \approx 0.04$-0.08 [11], while ARTI experiments by laser direct drive show lower values $\alpha_b \approx 0.04$ [26]. Recent ARTI experiments by indirect drive

TABLE I. Ablation reduces the RTI linear growth rate γ [1,30] while ablation-generated vorticity accelerates the nonlinear bubble velocity U_b [31–34]. Here k is the wave number. $r_d = \rho_l/\rho_h$ is the fluid density ratio. The coefficient $b = 3$-4 in the regime of interest. The geometry factor $C_g = 3$ in two dimensions and $C_g = 1$ for three dimensions. V_a is the ablation velocity. $\omega_0 \sim kV_a/r_d$ is the vorticity at the bubble vertex.

CRTI	ARTI
$\gamma = \sqrt{A_T kg}$	$\gamma = \sqrt{A_T kg} - bkV_a$
$U_b = \sqrt{g(1-r_d)/C_g k}$	$U_b = \sqrt{g(1-r_d)/C_g k + r_d \omega_0^2/4k^2}$

show that the multimode ARTI can grow faster than Haan's multimode model [27,28], suggesting that some nonlinear physics is missing in current understanding. Meanwhile, limited theoretical or numerical work on the self-similar multimode ARTI has been carried out with the exception of Refs. [14] and [16]. In both references, the ablation model only considers the ablative stabilization of the RTI linear growth rate but ignores the destabilization effect of the ablation-generated vorticity that accelerates the nonlinear bubble velocity (Table I). Recent studies also found that intense vorticity driven by finite amplitude perturbation can also destabilize all the linearly stable RTI modes beyond the nonlinear cutoff [29]. Because of the vorticity-driven nonlinear bubble acceleration, it seems that there is no general conclusion to whether mass ablation can suppress or enhance the nonlinear bubble-front penetration.

In this work, the multimode ARTI is studied numerically in great detail and compared with the classical case in both two and three dimensions. It is found that the nonlinear bubble penetration of the ARTI is dominated by bubble competition and α_b increases with the initial perturbation amplitude. The dependence of α_b on initial perturbation and ablation comes from the bubble competition theory, indicating that mass ablation can reduce α_b for the same initial perturbation amplitude. Furthermore, we show that while small scale perturbations reduce α_b in the CRTI by enhancing the bubble merger effect, they can enhance α_b in ARTI because of the vorticity-driven nonlinear bubble acceleration. Our results indicate that for sufficiently large initial perturbations, α_b in ARTI can be higher than in CRTI resulting in larger bubble growth than predicted by classical theory. The ARTI bubble competition theory can be applied in studies of ICF implosions and supernova explosions, which involve significant nonlinear ARTI phenomena.

The multimode ARTI simulations are carried out on a planar target using the hydrodynamic code ART [29,33,34]. ART solves the single fluid compressible inviscid equations of motion with Spitzer heat conduction and an ideal gas equation of state [35]. The equilibrium profile used in the multimode simulation is the same as in the single mode study in Ref. [29] [see Fig. 1(a) of Ref. [29]]. In the simulation, the heat flux is maintained in the Z direction to ablate the target with ablation velocity $V_a = 3.5\ \mu$m/ns. The heat flux is uniform in the X and Y directions. The initial acceleration $g_0 = 100\ \mu\text{m/ns}^2$ (typical values for direct drive ICF). Because of rocket acceleration, the density profile varies in space and $A_T \approx 1$. The linear cutoff wave number for the ARTI is $k_{cl} \approx 1\ \mu\text{m}^{-1}$. The RTI is seeded by velocity perturbations at the ablation front represented by $V_p(X) = \sum V_{pk} \cos(mk_L X + \phi_{k0})$ in two dimensions and by $V_p(X,Y) = V_{pk} \times \sum_{m,n} [\cos(mk_L X - nk_L Y) + 0.5 * \sum_{i=1}^4 \cos(mk_L X + nk_L Y + \phi_{mni})]$ in three dimensions. Here $k_L = 2\pi/L_X = 2\pi/L_Y$. L_X and L_Y are the length of the simulation domain in X and Y. m and n are the mode numbers in X and Y. The phase terms ϕ_{k0} and ϕ_{mni} are assigned randomly. The dependence of V_{pk} on Z is $V_{pk} = V_{pk0} \exp(k|Z - Z_0|)$ (Z_0 is the ablation front), which is the same as in Ref. [29]. The notation $Ps(m_1 - m_2)$ represents the power spectrum of the initial perturbation. Here $m_1 - m_2$ denotes the perturbed mode range and s denotes the spectrum index. For example, $P2(4\text{-}16)$ denotes the initial perturbation with modes $4k_L \le k \le 16k_L$ and each mode amplitude decays as k^{-2} with $k = k_L\sqrt{m^2 + n^2}$. The root-mean-square (rms) velocity $V_{\rm rms}$ normalized to $3.5\ \mu$m/ns represents the overall initial perturbation amplitude. In the multimode simulations, h_b is defined as the distance from the vertex of the fastest growing bubble to the initial ablation front in the frame of reference of the imploding shell. α_b is calculated by fitting the linear relation $h_b = \alpha_b S$ in the late-time nonlinear phase since $A_T \approx 1$ in the simulation. In our multimode simulations, the grid-cell size is $0.1\ \mu$m in each direction. The 2D simulations are carried out with $L_X = 100\,\mu$m while $L_X = L_Y = 50\ \mu$m is used in the 3D simulations. The simulation domain in the Z direction is $L_z = 110\ \mu$m for both two and three dimensions. In order to eliminate the effect of random perturbation phases, h_b is calculated by averaging over an ensemble of simulations with the same perturbation power spectrum but different random phases.

Figure 1(a) shows the nonlinear bubble penetration under different $V_{\rm rms}$ for the 2D multimode ARTI simulations with perturbation $P0(4\text{-}16)$. These perturbed modes

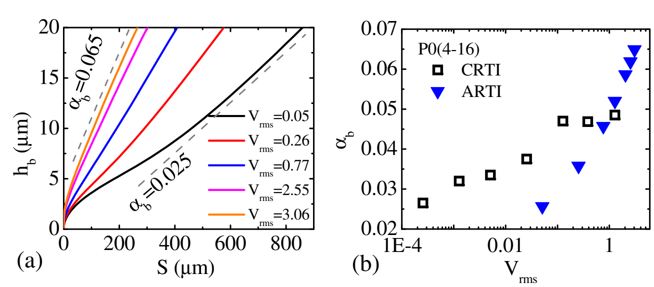

FIG. 1. (a) h_b vs S for the 2D ARTI simulations with different $V_{\rm rms}$. (b) Dependence of α_b on $V_{\rm rms}$ for both ARTI and CRTI simulations.

include wave numbers from the maximum linear growth rate to the linear cutoff. It is shown that h_b scales linearly with S in the nonlinear phase for all these simulations, indicating a self-similar nonlinear state. α_b increases with $V_{\rm rms}$ and varies from 0.025 to 0.065. For comparison, 2D multimode CRTI simulations are carried out with the same density profile and initial perturbation. In the absence of mass ablation, constant acceleration $g_0 = 100\ \mu\mathrm{m/ns}^2$ is used. As expected, h_b also scales linearly with S and α_b increases with $V_{\rm rms}$.

The dependence of α_b on $V_{\rm rms}$ is shown in Fig. 1(b) for both ARTI and CRTI simulations. In the CRTI simulations, α_b increases with $V_{\rm rms}$ when $V_{\rm rms}$ is small ($V_{\rm rms} < 0.1$), indicating that the nonlinear CRTI is dominated by bubble competition. This is consistent with the fact that the multimode amplitude grows exponentially in the linear phase before it reaches the self-similar state. When $V_{\rm rms}$ further increases ($V_{\rm rms} > 0.1$), the CRTI transits to the bubble merger regime with α_b independent of the initial perturbation. In contrast to CRTI, the ARTI is always in the bubble competition regime even when $V_{\rm rms}$ is large [Fig. 1(b)]. Because of the linear ablative stabilization, larger $V_{\rm rms}$ are required to reach the same α_b as in CRTI in the bubble competition regime. The simulations also show that the nonlinear bubble penetration of the ARTI can be faster (larger α_b) than in CRTI when $V_{\rm rms}$ is sufficiently large. This occurs because at large $V_{\rm rms}$, the ablation-generated vorticity enhances the bubble penetration by accelerating the nonlinear bubble velocity [33,34]. Because of the vorticity effect, the nonlinear ARTI does not transit to the bubble merger regime and α_b keeps increasing with $V_{\rm rms}$. It should be noted that in typical direct drive laser fusion experiments, the velocity perturbation around the ablation surface induced by laser speckles can easily exceed the ablation velocity, which may result in α_b being larger than in the classical case [29]. Similar dependence of α_b on initial perturbation is also found in 3D simulations discussed later.

To understand the effect of ablation on α_b, the relation between α_b and h_0 is derived for the ARTI. The ARTI linear dispersion relation (Table I) can be further written as $\gamma = \gamma_c(1 - b\hat{V}_a)$ with $\hat{V}_a = \sqrt{k/g}V_a$ the nondimensional ablation velocity (Table I) [30]. $\gamma_c = \sqrt{gk}$ is the CRTI linear growth rate in the $A_T = 1$ limit. Since the linear phase is short, we further assume that k and g are constant in the linear phase. Therefore, the bubble penetration distance h_b in the linear phase can be written as $h_b = h_0\exp(\gamma t) + V_a t$. The nonlinear phase develops at $t_{\rm NL}$ when $\partial h_b/\partial t = U_b = C\sqrt{g\lambda/2}$. The coefficient C is determined by the classical terminal bubble velocity U_b [10]. Here the vorticity terms are ignored for simplicity because vorticity is less effective on large size bubbles. Therefore, the nonlinear occurrence time and the correlated bubble penetration distance are $t_{\rm NL} = (1/\gamma)\ln\{[\sqrt{g/k}(C\sqrt{\pi} - \hat{V}_a)]/[h_0\gamma]\}$ and $h_b^{\rm NL} = h_0\exp(\gamma t_{\rm NL}) + V_a t_{\rm NL}$, respectively. At $t > t_{\rm NL}$, the fastest growing bubble evolves similarly to the single mode and the penetration distance satisfies $h_b = \int_{t_{\rm NL}}^t C\sqrt{g\lambda/2}dt + h_b^{\rm NL}$. Here λ is the wavelength of the fastest growing bubble. Applying the self-similar condition ($\partial h_b/\partial\lambda = 0$), we have $h_b \approx \alpha_b(\int\sqrt{g}dt)^2$ with $\alpha_b = [C\sqrt{\pi}(1 - b\hat{V}_a)/4]\times\{\ln[(C\sqrt{\pi} - \hat{V}_a)/(k_0h_0)/(1 - b\hat{V}_a)] - 1\}^{-1}$ for the ARTI. Since α_b depends weakly on the variables in the *ln* function and to make it more consistent with Eq. (1), the dependence of α_b on h_0 and V_a is rewritten as

$$\alpha_b \approx (1 - b\hat{V}_a)\alpha_{bC} = (1 - b\sqrt{k_0/g}V_a)\alpha_{bC}, \qquad (2)$$

where α_{bC} denotes the classical relation [Eq. (1)]. Equation (2) indicates that mass ablation can reduce α_b with respect to the classical value for the same initial perturbation in the bubble competition regime. The lower α_b in ARTI is due to the reduction of the linear growth rate by mass ablation. Similar relation between α_b and V_a was derived in the bubble merger model without the dependence of α_b on initial perturbation [16].

Equation (2) is further used to quantify the α_b dependence on h_0 and V_a for both 2D and 3D simulations. The initial surface perturbation h_0 in the simulation can be obtained by extrapolating the linear phase of the multimode amplitude to $t = 0$. $k_0 = 0.06$ is used to normalize h_0 for all the simulations. Figure 2(a) shows 2D simulation results for different V_a. The bubble competition regime of the 2D

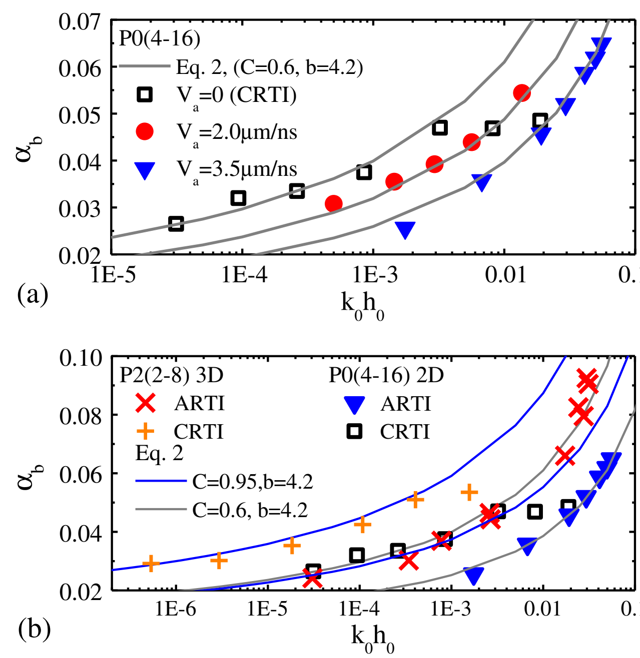

FIG. 2. (a) Dependence of α_b on h_0 for different ablation velocity. (b) Dependence of α_b on h_0 for 2D and 3D simulations with $V_a = 3.5\ \mu\mathrm{m/ns}$. In the 3D ARTI simulations, since α_b is quite sensitive to initial perturbation at large h_0, the simulation ensemble average of h_b is not required.

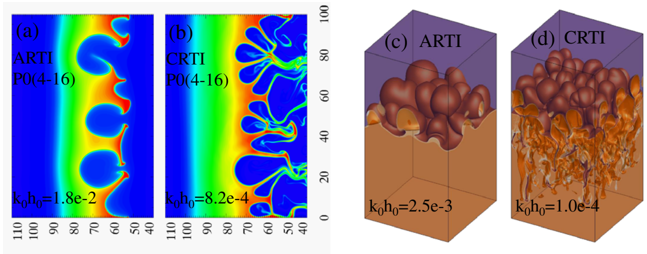

FIG. 3. Density contour plots in 2D simulations [(a) and (b)] and interface plots in 3D simulations [(c) and (d)] at deep nonlinear phase.

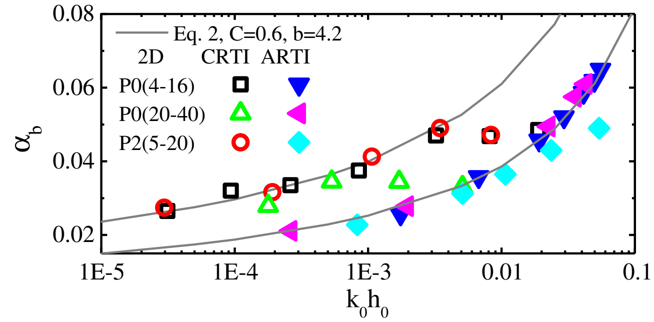

FIG. 4. The dependence of α_b on h_0 for different initial perturbation spectrum.

CRTI can be well fitted by Eq. (1) with $C = 0.6$. When the initial perturbation is significant, the CRTI transits to the bubble merger regime and α_b is insensitive to h_0 as shown by the saturation of the square dots in Fig. 2(a). Instead, all the 2D ARTI simulation results can be quantified by Eq. (2) with $b = 4.2$. In the bubble competition regime, linear ablative stabilization reduces α_b for the same h_0. However, the nonlinear ARTI can reach larger α_b values than in the classical case at large h_0 because it does not transit to the bubble merger regime. Figure 2(b) shows that α_b in 3D ARTI is higher than in two dimensions for the same h_0 and can reach even higher values at large h_0 because the 3D bubbles have higher bubble velocity and more intense vorticity [34]. Furthermore, the 3D simulations can also be represented by Eq. (2) with $C = 0.95$ and $b = 4.2$. The value of C in three dimensions is about 1.6 times larger than in two dimensions, consistent with the 3D classical terminal bubble velocity being 1.7 times larger than in two dimensions for the same wavelength [32]. It should also be noted that $C = 0.95$ in our 3D classical simulations is more consistent with the 3D CRTI experiments than $C = 0.56$ in the simulation of Refs. [10,25]. The value of b is the same in 2D and 3D simulations, indicating that the effect of ablation in reducing α_b is the same between 2D and 3D ARTI. This is consistent with the fact that the linear ablative stabilization is the same in two and three dimensions. Overall, the dependence of α_b on h_0 and V_a can be quantified by Eq. (2) for both 2D and 3D simulations. The 2D CRTI results are also confirmed by a different fluid code DiNuSUR [36].

Figure 3 shows the mode structure comparisons between the ARTI and CRTI simulations. In the 2D ARTI simulations, the bubble size is larger than in the CRTI. For the current perturbation spectrum, there are about 10 bubbles in the early nonlinear phase and 2–3 bubbles in the deep nonlinear phase [Fig. 3(a)], indicating that the nonlinear ARTI undergoes about 2 generations before the bubbles penetrate through the target. Because of mass ablation, the spikes are significantly suppressed and the late-time nonlinear phase is far from a turbulent state. Different from the ablative case, the 2D CRTI simulation has smaller bubble size and more complex spike structures in the deep nonlinear phase [Fig. 3(b)]. The 3D ARTI simulation [Fig. 3(c)] also has larger bubble size and shorter spikes compared to the classical case [Fig. 3(d)].

The vorticity effect on enhancing the ARTI nonlinear bubble penetration is shown in Fig. 4. Since vorticity effect is more significant for small scale perturbations, the dependence of α_b on h_0 is further investigated by 2D simulations using different initial perturbation spectrum. The perturbation $P2$(5-20) is dominated by large scale modes near $m = 5$ ($\lambda = 20\,\mu$m). The perturbation $P0$(20-40) is completely dominated by linearly stable small scale modes [Fig. 1(b)], which can be nonlinearly destabilized by finite amplitude perturbation and can be significantly affected by ablation-driven vorticity [29,33,34]. In the CRTI simulations, the relation between α_b and h_0 in $P2$(5-20) is quite similar to $P0$(4-16). Since only short wavelength perturbations are initialized in $P0$(20-40), the multimode CRTI transits to the bubble merger regime at much lower h_0 and $\alpha_b \approx 0.035$ is closer to its lower limit. The CRTI simulations show that significant small scale perturbations can suppress the nonlinear bubble penetration by enhancing the bubble merger effect. Instead, the perturbation P0(20-40) and P0(4-16) in the ARTI simulations have similar dependence of α_b on h_0. The perturbation $P2$(5-20) has slightly smaller α_b at large initial perturbation because the vorticity acceleration is less effective for larger size bubbles [33,34]. The perturbation $P0$(20-40) does not transit to the bubble merger region since small scale bubbles can be significantly accelerated by the vorticity effect thereby enhancing the nonlinear bubble growth. This result clearly shows that the ablation-generated vorticity can keep the nonlinear ARTI in the bubble competition region even for small scale initial perturbations. In the absence of vorticity, the small scale ARTI would behave like CRTI and transition from the bubble competition to the bubble merger regime, leading to the saturation of α_b. As a result, α_b in ARTI can reach higher value than in CRTI for sufficiently large initial perturbations.

In summary, numerical simulations of the 2D and 3D multimode ARTI show that the nonlinear ARTI is dominated by bubble competition and that mass ablation can reduce the ARTI nonlinear bubble growth with respect to the classical value for the same initial perturbation amplitude. The ablation-generated vorticity can accelerate the nonlinear bubble velocity and keep the nonlinear ARTI in the bubble competition regime, resulting in higher α_b value than in the classical case at large initial perturbation. Because of the dependence of α_b on initial perturbation and vorticity generation, ablative stabilization of the nonlinear ARTI is not as effective as previously anticipated for large initial perturbations. This theory can be used to explain the stability limits observed in direct drive ICF experiments [37] and details will be presented in an upcoming publication.

This work was supported by the DOE OFES Grant No. DE-SC0014318 and NNSA Grant No. DE-NA0001944. H. A. was also supported by NASA Grant No. 80NSSC18K0772 and by LANL Subcontract No. 482526. R. Y. was also supported by NSFC Grant No. 11772324 and Strategic Priority Research Program of the Chinese Academy of Science Grant No. XDB16. An award of computer time was provided by the INCITE program, using resources of the Argonne Leadership Computing Facility, which is a DOE Office of Science User Facility supported under Contract No. DE-AC02-06CH11357.

*zhang.huasen@gmail.com

[1] G. I. Taylor, Proc. R. Soc. A **201**, 192 (1950).
[2] L. Rayleigh, *Scientific Papers* (Cambridge University Press, Cambridge, England, 1900), Vol. II, p. 200.
[3] E. L. Blanton, T. E. Clarke, C. L. Sarazin, S. W. Randall, and B. R. McNamara, Proc. Natl. Acad. Sci. U.S.A. **107**, 7174 (2010).
[4] E. P. Hicks, Astrophys. J. **803**, 72 (2015).
[5] S. Atzeni and J. Meyer-ter-Vehn, *The Physics of Inertial Fusion: Beam Plasma Interaction Hydrodynamics, Hot Dense Mater* (Oxford University, Oxford, 2004).
[6] J. H. Gardner and S. E. Bodner, Phys. Rev. Lett. **47**, 1137 (1981).
[7] A. R. Bell, Mon. Not. R. Astron. Soc. **353**, 550 (2004).
[8] G. Dimonte and M. Schneider, Phys. Rev. E **54**, 3740 (1996).
[9] U. Alon, J. Hecht, D. Ofer, and D. Shvarts, Phys. Rev. Lett. **74**, 534 (1995).
[10] G. Dimonte, Phys. Rev. E **69**, 056305 (2004).
[11] G. Dimonte, D.L. Youngs, A. Dimits, S. Weber, M. Marinak, S. Wunsch, C. Garasi, A. Robinson, M. J. Andrews, P. Ramaprabhu *et al.*, Phys. Fluids **16**, 1668 (2004).
[12] V. N. Gamezo, A. M. Khokhlov, E. S. Oran, A. Y. Chtchelkanova, and R. O. Rosenberg, Science **299**, 77 (2003).
[13] T. Shigeyama and K. Nomoto, Astrophys. J. **360**, 242 (1990).
[14] S. W. Haan, Phys. Rev. A **39**, 5812 (1989).
[15] S. W. Haan, Phys. Fluids B **3**, 2349 (1991).
[16] D. Oron, U. Alon, and D. Shvarts, Phys. Plasmas **5**, 1467 (1998).
[17] R. Betti, K. Anderson, T. R. Boehly, T. J. B. Collins, R. S. Craxton, J. A. Delettrez, D. H. Edgell, R. Epstein, V. Y. Glebov, V. N. Goncharov *et al.*, Plasma Phys. Controlled Fusion **48**, B153 (2006).
[18] M. C. Herrmann, M. Tabak, and J. D. Lindl, Nucl. Fusion **41**, 99 (2001).
[19] J. Arons and S. M. Lea, Astrophys. J. **207**, 914 (1976).
[20] E. A. Frieman, Astrophys. J. **120**, 18 (1954).
[21] W. S. D. Wilcock and J. A. Whitehead, J. Geophys. Res. **96**, 12193 (1991).
[22] J. M. Finn, Phys. Fluids B **5**, 415 (1993).
[23] J. Glimm and D. Sharp, Phys. Rev. Lett. **64**, 2137 (1990).
[24] G. Dimonte, P. Ramaprabhu, D. L. Youngs, M. J. Andrews, and R. Rosner, Phys. Plasmas **12**, 056301 (2005).
[25] P. Paraprabhu, G. Dimonte, and M. J. Andrews, J. Fluid Mech. **536**, 285 (2005).
[26] O. Sadot, V. A. Smalyuk, J. A. Delettrez, D. D. Meyerhofer, T. C. Sangster, R. Betti, N. N. Goncharov, and D. Shvarts, Phys. Rev. Lett. **95**, 265001 (2005).
[27] D. A. Martinez, V. Z. Smalyuk, J. O. Kane, A. Casner, S. Liberatore, and L. P. Masse, Phys. Rev. Lett. **114**, 215004 (2015).
[28] A. Casner, L. Masse, S. Liberatore, P. Loiseau, P. E. Masson-Laborde, L. Jacquet, D. Martinez, A. S. Moore, R. Seugling, S. Felker *et al.*, Phys. Plasmas **22**, 056302 (2015).
[29] H. Zhang, R. Betti, V. Gopalaswamy, R. Yan, and H. Aluie, Phys. Rev. E **97**, 011203 (2018).
[30] H. Takabe, K. Mima, L. Montierth, and R. Morse, Phys. Fluids **28**, 3676 (1985).
[31] D. Layzer, Astrophys. J. **122**, 1 (1955).
[32] V. N. Goncharov, Phys. Rev. Lett. **88**, 134502 (2002).
[33] R. Betti and J. Sanz, Phys. Rev. Lett. **97**, 205002 (2006).
[34] R. Yan, R. Betti, J. Sanz, H. Aluie, B. Liu, and A. Frank, Phys. Plasmas **23**, 022701 (2016).
[35] J. Sanz, Phys. Rev. Lett. **73**, 2700 (1994).
[36] D. Zhao and H. Aluie, Phys. Rev. Fluids **3**, 054603 (2018).
[37] V. N. Goncharov, T. C. Sangster, R. Betti, T. R. Boehly, M. J. Bonino, T. J. B. Collins, R. S. Craxton, J. A. Delettrez, D. H. Edgell, R. Epstein *et al.*, Phys. Plasmas **21**, 056315 (2014).